ChemComm

COMMUNICATION

View Article Online
View Journal | View Issue

Cite this: *Chem. Commun.*, 2018, **54**, 2792

Received 20th December 2017,
Accepted 22nd February 2018

DOI: 10.1039/c7cc09739e

rsc.li/chemcomm

Enhancing anticancer cytotoxicity through bimodal drug delivery from ultrasmall Zr MOF nanoparticles†

Isabel Abánades Lázaro, Sandra Abánades Lázaro and Ross S. Forgan *

Dual delivery of dichloroacetate and 5-fluorouracil from Zr MOFs into cancer cells is found to enhance *in vitro* cytotoxicity. Tuning particle size and, more significantly, surface chemistry, further improves cytotoxicity by promoting caveolae-mediated endocytosis and cytosolic cargo delivery.

Effective cell internalisation and intracellular drug release are vital characteristics of effective nanoparticulate drug delivery systems (DDSs).[1] Nanoparticles are generally internalised through active transport mechanisms such as endocytosis, however, if they are small enough (<20 nm), nanoparticles can be internalised by passive diffusion,[2] enabling direct release of cargo into the cytosol. Metal–organic frameworks (MOFs)[3] – network structures composed of metal clusters linked by multidentate organic linkers with high porosity – offer the desirable combination of large cargo payloads and tunable structural features,[4] with zirconium MOFs,[5] which have requisite chemical stability for aqueous use, emerging as promising potential DDSs.[6]

We have previously shown[7] that 50–600 nm nanoparticles of UiO-66, the zirconium 1,4-benzenedicarboxylate (bdc) MOF with ideal formula $[Zr_6O_4(OH)_4(bdc)_6]_n$, and its –Br, $-NO_2$, and $-NH_2$ functionalised derivatives (**L1–L4** in Fig. 1a), undergo HeLa cancer cell internalisation primarily through clathrin-mediated endocytosis, while isoreticular MOFs with more hydrophobic extended linkers, such as 2,6-napthalenedicarboxylate (**L5**) and 4,4′-biphenyldicarboxylate (**L6**), are partially internalised through caveolae-mediated endocytosis, with no induction of cytotoxicity at concentrations up to 1 mg mL^{-1}.[8] Similarly, coating surfaces of UiO-66 nanoparticles with poly(ethylene glycol) can promote caveolae-mediated uptake, allowing drug-loaded MOFs to avoid the lysosomal degradation that is characteristic of clathrin-mediated endocytosis and release their cargo in the cytosol, thus enhancing therapeutic efficiency.[9]

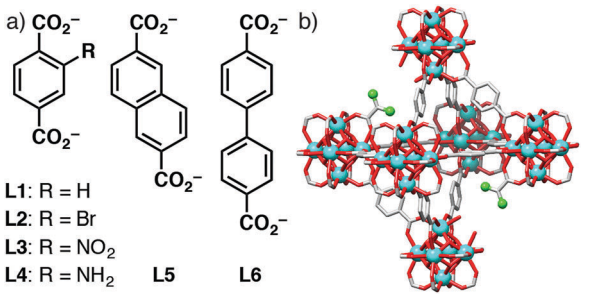

Fig. 1 (a) Structures of linkers **L1–L6** used in the preparation of all **Zr-LX** MOFs. (b) Schematic of DCA@**Zr-L1** with DCA capping Zr_6 clusters to form defects.

This example utilised the anticancer metabolic molecule, dichloroacetic acid (DCA), as a modulator[10] of UiO-66 solvothermal synthesis, showing that it can be incorporated into UiO-66 nanoparticles at defects and on their surfaces (Fig. 1b), yielding regular, well-dispersed, porous nanoparticles of around 100 nm in size.[9] Herein, we (i) investigate the DCA modulation protocol across the isoreticular series of Zr MOFs illustrated in Fig. 1, (ii) show that very small (*ca.* 20 nm), highly defective, DCA-containing Zr MOFs can be prepared and loaded with a second anticancer drug, and (iii) demonstrate enhanced *in vitro* cancer cell cytoxicity of the dually active DDSs.

DCA is a pyruvate D-kinase inhibitor, which is over expressed in cancerous cells, and its cytotoxic effects on cancer cells depend on effective cytosolic release and mitochondrial localisation, thus making it an ideal mechanistic probe molecule for cell uptake.[11] To promote cytosolic release through passive diffusion, we have tuned our previously reported synthetic conditions for DCA@**Zr-L1** with the aim of obtaining smaller, DCA-loaded nanoparticles (<20 nm) of the MOFs **Zr-L1**–**Zr-L6** (ESI,† Section S2). Solvothermal reaction of $ZrOCl_2$ with 2.5 eq. of linker and 18.2 eq. of dichloroacetic acid yields solids whose powder X-ray diffraction (PXRD) patterns (Fig. 2a) show Bragg peaks characteristic of the UiO-66 topology.[5a] When terephthalate linkers (**L1** to **L4**) are used, the diffraction patterns have broad, low intensity peaks, suggesting

WestCHEM, School of Chemistry, University of Glasgow, University Avenue, Glasgow, G12 8QQ, UK. E-mail: Ross.Forgan@glasgow.ac.uk

† Electronic supplementary information (ESI) available: MOF synthesis, analysis and *in vitro* testing. See DOI: 10.1039/c7cc09739e

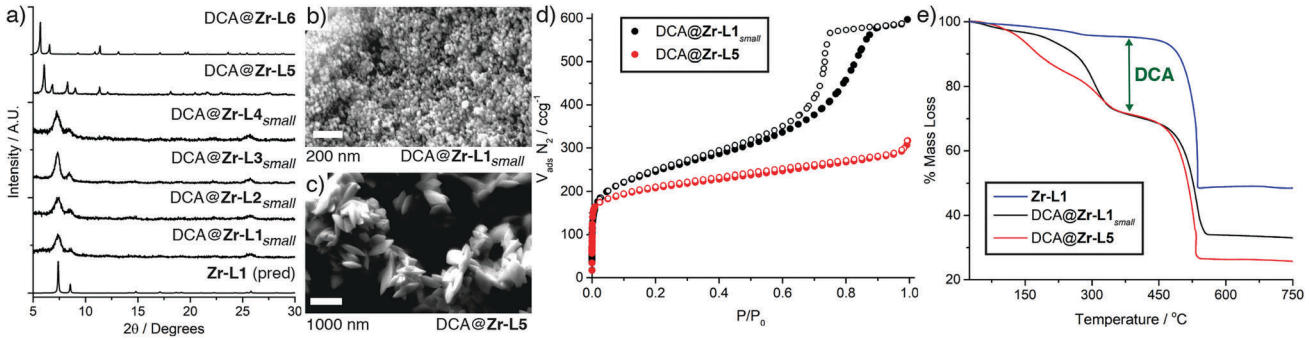

Fig. 2 (a) Stacked PXRD patterns of DCA@MOFs. SEM images of (b) DCA@**Zr-L1**$_{small}$ (~20 nm) and (c) DCA@**Zr-L5** (~230 nm). (d) N_2 uptake isotherms (77 K) of DCA@**Zr-L1**$_{small}$ and DCA@**Zr-L5**. Filled symbols represent adsorption, empty symbols desorption. (e) TGA traces of DCA@**Zr-L1**$_{small}$ and DCA@**Zr-L5** compared to pristine **Zr-L1**.

small and defective particles, as a consequence of DCA attachment to the Zr_6 clusters in place of linkers.[12]

Scanning electron microscopy (SEM) confirms that the zirconium terephthalates form as 10–30 nm particles, which are termed DCA@**Zr-LX**$_{small}$ to denote the small particle size; DCA@**Zr-L1**$_{small}$ is shown as an exemplar in Fig. 2b. In contrast, DCA@**Zr-L5** nanoparticles have an unexpected ovoid morphology (Fig. 2c) with diameters of 232 ± 30 nm and lengths about 700 nm, which, combined with additional reflections in the PXRD pattern, suggests a defective, lower connectivity structure that has been observed with acetic acid modulated analogues.[13] DCA@**Zr-L6** is composed of polycrystalline spherical nanoparticles of 196 ± 32 nm in size (Fig. S4, ESI†).

The terephthalate MOFs present type IV N_2 adsorption and desorption isotherms (77 K) with H2 hysteresis loops typical of interconnected networks of pores with different size and shape[14] (illustrated for DCA@**Zr-L1**$_{small}$ in Fig. 2d). These suggest highly defective structures, although some contribution of inter-particle space should be considered. The BET surface areas are lower than defect-free UiO-66 (1200 $m^2\ g^{-1}$),[5a] but the additional, defect-induced mesoporosity results in extremely high pore volumes, ranging from 0.8 to 1.2 cc g^{-1}. DCA@**Zr-L5** (Fig. 2d) and DCA@**Zr-L6** (Fig. S7, ESI†) are also porous but do not exhibit hysteresis, in concert with PXRD and SEM analysis that indicate larger, less defective particles. The BET surface areas and pore volumes are given in Table 1.

Nuclear magnetic resonance (NMR) spectra of acid-digested samples confirm significant incorporation of DCA, while FT-IR spectra show appearance of vibration bands characteristic of DCA, but shifted to indicate its attachment at defect sites (ESI,† Section S2). Thermogravimetric analysis (TGA) of the DCA@MOFs shows significant mass loss events from 250–375 °C compared to pristine materials (Fig. 2e and Fig. S11, ESI†), allowing quantification of DCA content (Table 1). Analogous terephthalate DCA@MOFs of larger size (*ca.* 100 nm) were also synthesised as size controls following our previously reported protocol.[9] Full characterisation (ESI,† Section S3) showed the samples (named DCA@**Zr-LX**) to be crystalline, porous, and contain significant quantities of DCA at defect sites, albeit in lower quantities than the smaller particles. Defect loading of drugs offers potential slow release of molecules bonded to the Zr_6 SBUs while maintaining both porosity, for introduction of further drugs, and stability, to allow subsequent postsynthetic functionalisation.[9]

Incorporation of modulators with low pK_a values into Zr MOFs is known to induce higher surface charge and thus enhance dispersion in water.[15] Dynamic light scattering (DLS, Section S4, ESI†) measurements (0.1 mg mL^{-1} in water) showed some aggregation of the smaller samples; DCA@**Zr-L1**$_{small}$, DCA@**Zr-L2**$_{small}$ and DCA@**Zr-L3**$_{small}$ form stable aggregates of ~250 nm, while the average size of DCA@**Zr-L4**$_{small}$ aggregates is ~75 nm, closer to the size determined by SEM. Positive surface charge from the protonated amino units of **L4** may decrease aggregation. Of the larger particles, only DCA@**Zr-L3** (~350 nm) and DCA@**Zr-L6** (~550 nm) show any notable deviation from the SEM particle size analyses. Nanoparticles are known to be further stabilised by the formation of a surface protein corona,[8,16] hence, when the smaller MOFs were dispersed in phosphate buffered saline (pH = 7.4) spiked with 2% *w*/*w* bovine serum album, their aggregation drastically decreased, with particle sizes close to the

Table 1 Pertinent physical characteristics of the DCA@MOFs

	Size/nm (SEM)	% DCA *w*/*w*	BET SA/$m^2\ g^{-1}$	Pore vol/cc g^{-1}	% 5-FU[a] *w*/*w*
DCA@**Zr-L1**$_{small}$	12.8 ± 3.6	26.2	891	0.87	1.9
DCA@**Zr-L2**$_{small}$	30.2 ± 7.9	19.3	639	0.81	3.8
DCA@**Zr-L3**$_{small}$	21.7 ± 5.3	21.5	901	1.12	4.3
DCA@**Zr-L4**$_{small}$	12.5 ± 2.9	26.4	990	1.21	2.4
DCA@**Zr-L5**	232 ± 30	14.1	764	0.42	1.5
DCA@**Zr-L6**	196 ± 32	6.6	2241	0.99	2.5

[a] Determined after postsynthetically loading 5-FU into the DCA@MOF sample.

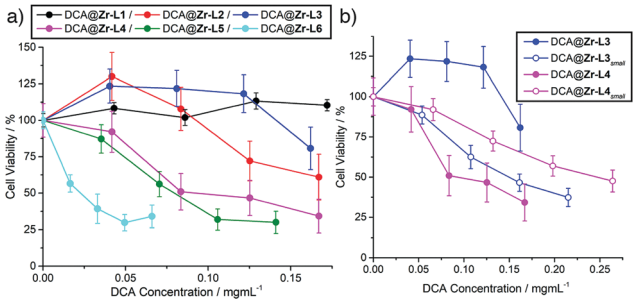

Fig. 3 (a) MCF-7 cell proliferation on incubation with the larger DCA@MOFs. Exact cell viability values are tabulated in the supporting information alongside plots against MOF concentration. (b) Comparison of MCF-7 cell proliferation for smaller and larger DCA@**Zr-L3** and DCA@**Zr-L4** samples.

ones determined by SEM for the positively charged DCA@**Zr-L4**$_{small}$ and aggregates of ~100 nm for the rest of the smaller MOFs. Aggregation of DCA@**Zr-L6** (~200 nm) also decreased.

The cytotoxicity of the DCA@MOFs towards MCF-7 breast cancer cells was assessed using the MTS cell proliferation assay (ESI,† Section S5). Free DCA has little effect on cell proliferation, as its hydrophilic nature results in poor internalisation;[17] a decrease in cell viability was observed only for concentrations >3 mg mL^{-1} (Fig. S28, ESI†). To examine the effect of ligand functionality, the cytotoxicities of the larger DCA-containing terephthalate derivatives (*ca.* 70–130 nm) were compared with DCA@**Zr-L5** and DCA@**Zr-L6** (*ca.* 200 nm), and plotted against DCA concentration (Fig. 3a). DCA@**Zr-L5** and DCA@**Zr-L6** are most therapeutically active, decreasing MCF-7 viabilities to around 35% when delivering <0.1 mg mL^{-1} of DCA. These results correlate well with the enhanced cytotoxicity towards HeLa cancer cells of **Zr-L6** when delivering the anti-cancer drug α-cyano-4-hydroxycinnamic acid,[8] likely as a consequence of the preference of **Zr-L5** and **Zr-L6** for caveolae-mediated endocytosis promoting efficient cytosolic cargo release,[7] rather than size, as empty **Zr-L5** and **Zr-L6** samples of varying size were found to not be cytotoxic towards HeLa cells.[8]

DCA@**Zr-L1**, in contrast, shows no cytotoxicity towards MCF-7, likely due to clathrin-mediated endocytosis leading to lysosome localisation; our previous work showed that a similar material has no cytotoxicity towards HeLa cells at similar concentrations.[9] DCA@**Zr-L2** and DCA@**Zr-L3** only reduce proliferation to 61 ± 16% and 81 ± 15%, respectively, at the highest delivered DCA concentrations, while the enhanced therapeutic effect of DCA@**Zr-L4**, with cell viabilities similar to DCA@**Zr-L5**, could be a result of the positive surface charge of protonated amino units in **L4** enhancing internalisation efficiency.[18] The effect of particle size was assessed by comparing the cytotoxicities of the DCA@**Zr-LX**$_{small}$ derivatives (~20 nm) towards MCF-7 cells with their larger DCA@**Zr-LX** analogues (~100 nm), and generally the smaller nanoparticles showed enhanced cytotoxicity when plotted against DCA concentration, suggesting enhanced internalisation and cell uptake by passive diffusion resulting in cytosolic release.[18b] Fig. 3b shows the more pronounced cytotoxicity of DCA@**Zr-L3**$_{small}$ compared to its larger analogue, which shows no appreciable deleterious effects, with similar trends observed for DCA@**Zr-L1**$_{small}$ and DCA@**Zr-L2**$_{small}$ (Fig. S31, ESI†). Only DCA@**Zr-L4**$_{small}$ (*ca.* 13 nm) was less efficient than its larger analogue DCA@**Zr-L4** (*ca.* 86 nm), but both samples still reduced cell proliferation, again likely due to their surfaces having significant positive charge.

It has been reported that DCA enhances the cytotoxic activity of anticancer drugs such as 5-fluorouracil (5-FU) while reducing cancer cells' resistance towards them.[17b,19] As such, the smaller, DCA-loaded terephthalate MOF samples that had shown generally enhanced cytotoxicity, along with DCA@**Zr-L5** and DCA@**Zr-L6**, were postsynthetically loaded with 5-FU to generate multimodal DDSs (ESI,† Section S6). Thermogravimetric analysis cannot distinguish between loaded DCA and 5-FU, although it suggests some loss of DCA during 5-FU loading for the small terephthalate MOFs. The loading of 5-FU, shown in Table 1, was calculated by UV-Vis spectroscopy, and found to range from 1.5–4.3% *w*/*w*.

The enhanced cytotoxicity (ESI,† Section S7) of all the 5-FU@DCA@MOFs towards MCF-7 cells compared to their DCA@MOF precursors, despite the decrease in DCA content, is clearly observed when cell proliferation is plotted against MOF concentration (Fig. 4a) suggesting successful intracellular deliver of 5-FU. Of the smaller MOF species, 5-FU@DCA@**Zr-L1**$_{small}$ exhibits a more significant dose–response effect than its precursor, decreasing cell viability with concentration down to 21 ± 7% at 1 mg mL^{-1}. The cytotoxicity of 5-FU@DCA@**Zr-L2**$_{small}$ increases only slightly compared to its precursor, whereas 5-FU@DCA@**Zr-L3**$_{small}$ and 5-FU@DCA@**Zr-L4**$_{small}$ have more notable enhancements, with cell viabilities of 19 ± 7% and 33 ± 8%, respectively, when MCF-7 cells were incubated with 0.5 mg mL^{-1} of the MOFs.

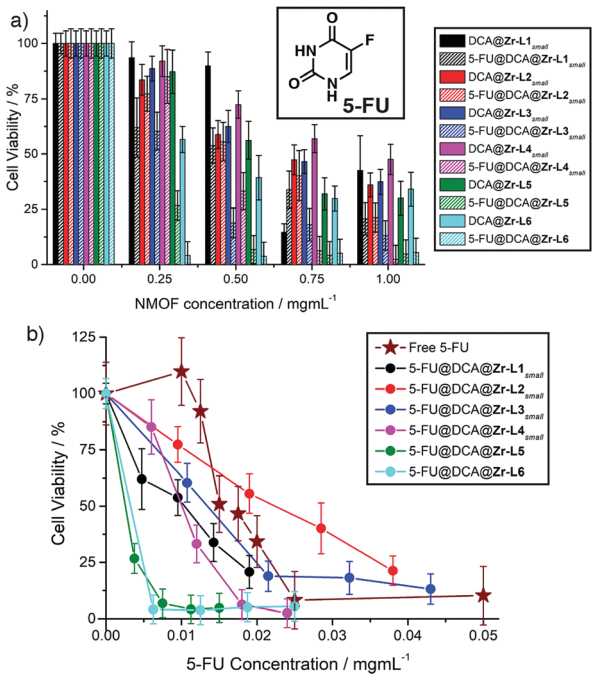

Fig. 4 (a) Comparison of MCF-7 cell proliferation on incubation with DCA@MOFs *versus* 5-FU@DCA@MOFs. (b) Comparison of activities of 5-FU@DCA@MOFs plotted against 5-FU concentration. Exact cell viability values are tabulated in the ESI.†

The most effective of the DCA@MOFs also showed further enhancements in cytotoxicity towards MCF-7 cells when loaded with 5-FU; cell viability drastically decreases to values of $7 \pm 6\%$ and $4 \pm 6\%$ when cells were incubated with just 0.5 mg mL^{-1} of 5-FU@DCA@**Zr-L5** and 5-FU@DCA@**Zr-L6**, respectively.

Free 5-FU itself also has significant dose-responsive cytotoxic behaviour (Fig. 4b), with an IC_{50} of 0.015 ± 0.001 mg mL^{-1}, but plotting cytotoxicity of the 5-FU@DCA@MOF samples against 5-FU concentration shows they have a greater effect than the free drug at lower concentrations, which might be a consequence of more efficient or faster internalisation, or a synergistic effect of DCA and 5-FU delivered in tandem, given that the cytotoxicity of free 5-FU is not enhanced when administered with DCA (Fig. S36, ESI†). At higher concentrations 5-FU@DCA@**Zr-L1$_{small}$** and 5-FU@DCA@**Zr-L4$_{small}$** continue to exhibit greater cytotoxic effects than the free drug, while 5-FU@DCA@**Zr-L3$_{small}$** has no notable enhancement and 5-FU@DCA@**Zr-L2$_{small}$** has a poorer performance than free 5-FU. Again, the larger samples, 5-FU@DCA@**Zr-L5** and 5-FU@DCA@**Zr-L6** have the most pronounced cytotoxic effects, significantly enhancing the efficacy of free 5-FU and killing nearly all cells at all measured concentrations, suggesting that it is the surface chemistry of the MOFs that influences cellular uptake, and thus cytotoxicity, to a greater extent.

We have shown that incorporation of DCA at defect sites during the modulated synthesis of Zr MOFs offers (i) particle size control in the assembly of highly defective $\sim$20 nm nanoparticles of hierarchically porous materials, (ii) high loading (15–25% *w*/*w*) of the anticancer probe molecule DCA, and (iii) porous MOFs into which further medicinal cargo can be loaded. On the whole, the smaller ($\sim$20 nm) DCA-loaded particles exhibit greater cytotoxicity towards MCF-7 cancer cells than their larger ($\sim$100 nm) analogues; we hypothesise that partial internalisation of the smaller MOFs through passive diffusion allows DCA release directly into the cytosol to enhance its therapeutic effects. However, the surface chemistry of the MOFs has a greater effect, with DCA@**Zr-L5** and DCA@**Zr-L6** the most therapeutically efficient MOFs, despite their bigger size, in agreement with our recent study on endocytosis mechanisms.[7] Concurrent delivery of two drugs from the 5-FU@DCA@MOFs further enhances cytotoxicity compared to precursor DCA@MOFs and the free drugs. Delivery of multiple drugs from one DDS has the potential to overcome issues with resistance and poor efficacy, and is enabled by utilisation of different loading protocols; defect-loading of cargo into Zr MOFs is possible for any carboxylic acid containing drug.

RSF thanks the Royal Society for a URF and the University of Glasgow for funding.

Conflicts of interest

There are no conflicts to declare.

Notes and references

1 (*a*) T.-G. Iversen, T. Skotland and K. Sandvig, *Nano Today*, 2011, **6**, 176–185; (*b*) I. Canton and G. Battaglia, *Chem. Soc. Rev.*, 2012, **41**, 2718–2739.
2 L. Treuel, X. Jiang and G. U. Nienhaus, *J. R. Soc., Interface*, 2013, **10**, 20120939.
3 H. Furukawa, K. E. Cordova, M. O'Keeffe and O. M. Yaghi, *Science*, 2013, **341**, 1230444.
4 P. Horcajada, R. Gref, T. Baati, P. K. Allan, G. Maurin, P. Couvreur, G. Férey, R. E. Morris and C. Serre, *Chem. Rev.*, 2012, **112**, 1232–1268.
5 (*a*) J. H. Cavka, S. Jakobsen, U. Olsbye, N. Guillou, C. Lamberti, S. Bordiga and K. P. Lillerud, *J. Am. Chem. Soc.*, 2008, **130**, 13850–13851; (*b*) Y. Bai, Y. Dou, L.-H. Xie, W. Rutledge, J.-R. Li and H.-C. Zhou, *Chem. Soc. Rev.*, 2016, **45**, 2327–2367.
6 (*a*) X. Zhu, J. Gu, Y. Wang, B. Li, Y. Li, W. Zhao and J. Shi, *Chem. Commun.*, 2014, **50**, 8779–8782; (*b*) C. He, K. Lu, D. Liu and W. Lin, *J. Am. Chem. Soc.*, 2014, **136**, 5181–5184; (*c*) D. Chen, D. Yang, C. A. Dougherty, W. Lu, H. Wu, X. He, T. Cai, M. E. Van Dort, B. D. Ross and H. Hong, *ACS Nano*, 2017, **11**, 4315–4327; (*d*) R. Röder, T. Preiß, P. Hirschle, B. Steinborn, A. Zimpel, M. Höhn, J. O. Rädler, T. Bein, E. Wagner, S. Wuttke and U. Lächelt, *J. Am. Chem. Soc.*, 2017, **139**, 2359–2368; (*e*) M. H. Teplensky, M. Fantham, P. Li, T. C. Wang, J. P. Mehta, L. J. Young, P. Z. Moghadam, J. T. Hupp, O. K. Farha, C. F. Kaminski and D. Fairen-Jimenez, *J. Am. Chem. Soc.*, 2017, **139**, 7522–7532.
7 C. Orellana-Tavra, S. Haddad, R. J. Marshall, I. Abánades Lázaro, G. Boix, I. Imaz, D. Maspoch, R. S. Forgan and D. Fairen-Jimenez, *ACS Appl. Mater. Interfaces*, 2017, **9**, 35516–35525.
8 C. Orellana-Tavra, R. J. Marshall, E. F. Baxter, I. A. Lazaro, A. Tao, A. K. Cheetham, R. S. Forgan and D. Fairen-Jimenez, *J. Mater. Chem. B*, 2016, **4**, 7697–7707.
9 I. Abánades Lázaro, S. Haddad, S. Sacca, C. Orellana-Tavra, D. Fairen-Jimenez and R. S. Forgan, *Chem*, 2017, **2**, 561–578.
10 (*a*) A. Schaate, P. Roy, A. Godt, J. Lippke, F. Waltz, M. Wiebcke and P. Behrens, *Chem. – Eur. J.*, 2011, **17**, 6643–6651; (*b*) C. V. McGuire and R. S. Forgan, *Chem. Commun.*, 2015, **51**, 5199–5217.
11 (*a*) E. D. Michelakis, L. Webster and J. R. Mackey, *Br. J. Cancer*, 2008, **99**, 989–994; (*b*) E. D. Michelakis, G. Sutendra, P. Dromparis, L. Webster, A. Haromy, E. Niven, C. Maguire, T. L. Gammer, J. R. Mackey, D. Fulton, B. Abdulkarim, M. S. McMurtry and K. C. Petruk, *Sci. Transl. Med.*, 2010, **2**, 31ra34; (*c*) D. Heshe, S. Hoogestraat, C. Brauckmann, U. Karst, J. Boos and C. Lanvers-Kaminsky, *Cancer Chemother. Pharmacol.*, 2011, **67**, 647–655.
12 (*a*) M. Taddei, K. C. Dumbgen, J. A. van Bokhoven and M. Ranocchiari, *Chem. Commun.*, 2016, **52**, 6411–6414; (*b*) B. Bueken, N. Van Velthoven, T. Willhammar, T. Stassin, I. Stassen, D. A. Keen, G. V. Baron, J. F. M. Denayer, R. Ameloot, S. Bals, D. De Vos and T. D. Bennett, *Chem. Sci.*, 2017, **8**, 3939–3948.
13 V. Bon, I. Senkovska, M. S. Weiss and S. Kaskel, *CrystEngComm*, 2013, **15**, 9572–9577.
14 F. Rouquerol, J. Rouquerol and K. Sing, in *Adsorption by Powders and Porous Solids*, Academic Press, London, 1999, 191–217.
15 W. Morris, S. Wang, D. Cho, E. Auyeung, P. Li, O. K. Farha and C. A. Mirkin, *ACS Appl. Mater. Interfaces*, 2017, **9**, 33413–33418.
16 (*a*) E. Bellido, M. Guillevic, T. Hidalgo, M. J. Santander-Ortega, C. Serre and P. Horcajada, *Langmuir*, 2014, **30**, 5911–5920; (*b*) E. Bellido, T. Hidalgo, M. V. Lozano, M. Guillevic, R. Simón-Vázquez, M. J. Santander-Ortega, Á. González-Fernández, C. Serre, M. J. Alonso and P. Horcajada, *Adv. Healthcare Mater.*, 2015, **4**, 1246–1257.
17 (*a*) C. Trapella, R. Voltan, E. Melloni, V. Tisato, C. Celeghini, S. Bianco, A. Fantinati, S. Salvadori, R. Guerrini, P. Secchiero and G. Zauli, *J. Med. Chem.*, 2016, **59**, 147–156; (*b*) J. Zajac, H. Kostrhunova, V. Novohradsky, O. Vrana, R. Raveendran, D. Gibson, J. Kasparkova and V. Brabec, *J. Inorg. Biochem.*, 2016, **156**, 89–97.
18 (*a*) A. M. Bannunah, D. Vllasaliu, J. Lord and S. Stolnik, *Mol. Pharmaceutics*, 2014, **11**, 4363–4373; (*b*) K. Yin Win and S.-S. Feng, *Biomaterials*, 2005, **26**, 2713–2722.
19 Y. Xuan, H. Hur, I.-H. Ham, J. Yun, J.-Y. Lee, W. Shim, Y. B. Kim, G. Lee, S.-U. Han and Y. K. Cho, *Exp. Cell Res.*, 2014, **321**, 219–230.